Journal of Computational Physics 347 (2017) 416–436

Contents lists available at ScienceDirect

Journal of Computational Physics

www.elsevier.com/locate/jcp

Approximate static condensation algorithm for solving multi-material diffusion problems on meshes non-aligned with material interfaces

Evgeny Kikinzon [a,*], Yuri Kuznetsov [b], Konstatin Lipnikov [a], Mikhail Shashkov [c]

[a] Applied Mathematics and Plasma Physics, T-5, Los Alamos National Laboratory, MS B284, Los Alamos, NM 87545, USA
[b] University of Houston, Department of Mathematics, 641 PGH, Houston, TX 77204, USA
[c] Methods and Algorithms, XCP-4, Los Alamos National Laboratory, MS F644, Los Alamos, NM 87545, USA

ARTICLE INFO

Article history:
Received 27 March 2017
Received in revised form 27 June 2017
Accepted 30 June 2017
Available online 8 July 2017

Keywords:
Multi-material problems
Diffusion equations
Numerical methods for PDEs

ABSTRACT

In this paper, we describe a new algorithm for solving multi-material diffusion problem when material interfaces are not aligned with the mesh. In this case interface reconstruction methods are used to construct approximate representation of interfaces between materials. They produce so-called multi-material cells, in which materials are represented by material polygons that contain only one material. The reconstructed interface is not continuous between cells. We suggest the new method for solving multi-material diffusion problems on such meshes and compare its performance with known homogenization methods.

Published by Elsevier Inc.

1. Introduction and rationale

The real world problems are multi-material and materials usually have very different properties: gases, liquids and solids. The material interfaces may be fixed in time or can be a part of the solution as in fluid-structure interactions or dynamics of air bubbles in water. In the latter case, interfaces can move and change shape, resulting in a possible change of connectivity.

In this paper we focus on solving the multi-material diffusion-type problems such as heat conduction or flow in porous media. Different materials occupy different parts of the computational domain and are separated by distinct material interfaces. Each sub-domain occupied by a single material has specific values of problem parameters associated with it. On material interfaces, special conditions (e.g., continuity of temperature and normal component of flux for heat conduction equations) have to be satisfied and taken into account in a discretization process. The fundamental laws of physics such as the conservation of energy (for heat conduction) and conservation of mass (for flow in porous media) must hold on a discrete level.

The applications targeted for impact require numerical methods that work on general polytopal (polyhedral in 3D and polygonal in 2D) meshes with potentially non-convex cells. In such applications the computational mesh may be non-conformal to interfaces due to complexity of these interfaces, presence of small fractions of materials, or because the mesh moves arbitrary with respect to the flow, as in the arbitrary Lagrangian–Eulerian (ALE) methods, [7,5].

A mesh that is non-conformal to material interfaces consists of pure cells, which contain only one material, and multi-material cells (MMCs), which contain two or more different materials (e.g. air, water and metal). In practice, the complexity

* Corresponding author.
E-mail addresses: kikinzon@lanl.gov (E. Kikinzon), kuz@math.uh.edu (Y. Kuznetsov), lipnikov@lanl.gov (K. Lipnikov), shashkov@lanl.gov (M. Shashkov).

http://dx.doi.org/10.1016/j.jcp.2017.06.048
0021-9991/Published by Elsevier Inc.

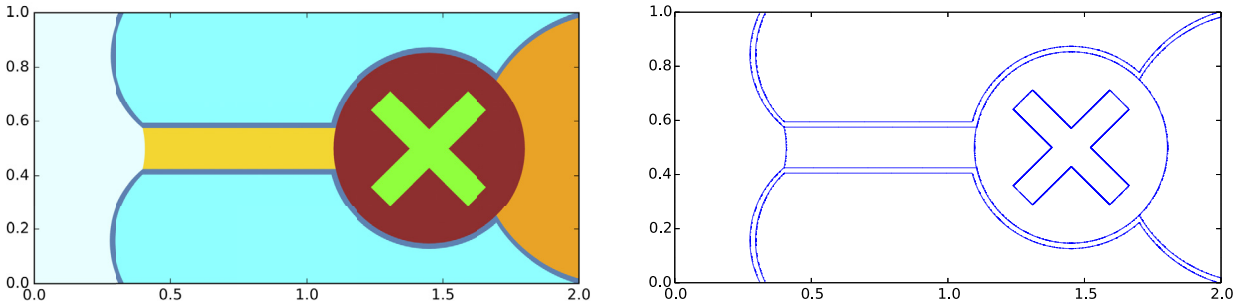

Fig. 1. Domain Ω containing seven materials distributed over nine subdomains Ω_i, including two thin material layers shown in blue; left – materials colored by different colors, right – interfaces. (For interpretation of the references to color in this figure, the reader is referred to the web version of this article.)

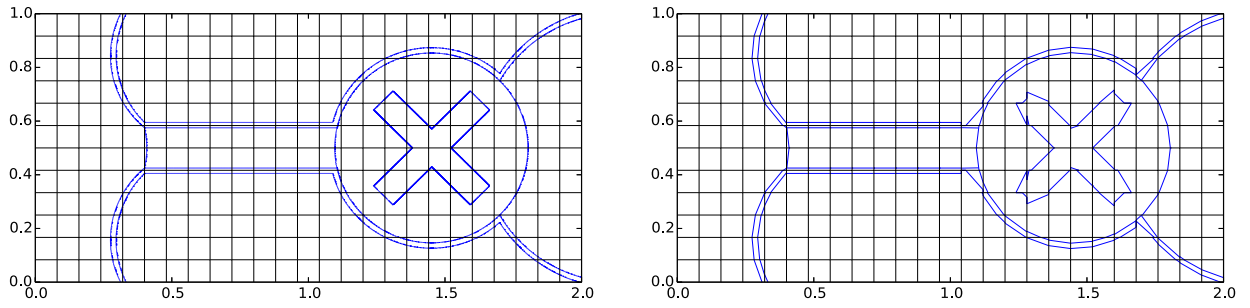

Fig. 2. An example of a mesh with multi-material cells: left – domain Ω with a superimposed "base" mesh Ω_h; right – reconstructed interfaces between materials for Ω_h, which are not a part of Ω_h.

of multi-physics problems that we have to solve and spatial resolution that computers are capable to deal with lead to cases where an MMC may contain up to ten materials. Many real materials may have tensorial material properties, like thermal conductivity.

In this paper we introduce a new method for solving multi-material diffusion-type equations on general polygonal meshes containing MMCs.

Let us consider computational domain in Fig. 1. It contains seven different materials distributed over nine subdomains, and the properties of these materials can be very different and discontinuous across material interfaces. Let us consider a linear non-stationary multi-material diffusion equation

$$\rho c_p \frac{\partial T}{\partial t} - \nabla \cdot (\mathbf{K} \nabla T) = f \,, \tag{1}$$

where T is a temperature, ρ – density, c_p – specific heat capacity, $\mathbf{K}$ – tensor of thermal conductivity, which can be a general symmetric positive definite tensor. This equation is valid in subdomains Ω_i containing a single material. On material interfaces, temperature, T, and normal component of flux are required to be continuous:

$$[T]_{ij} = 0 \quad \text{and} \quad [(\mathbf{K} \nabla T) \cdot \mathbf{n}]_{ij} = 0 \,, \tag{2}$$

where Γ_{ij} is the interface between materials i and j, $\mathbf{n}$ is the unit normal, and $[p]_{ij}$ is the jump in p over the interface Γ_{ij}.

We assume that the computational domain is covered by a mesh, which we will call the *base* mesh – left panel in Fig. 2. In general, a base mesh will not be aligned with material interfaces. In ALE methods the mesh is moving arbitrarily, and even if calculations start on a mesh aligned with material interfaces, eventually the mesh and the material interfaces will not be aligned. It is also important to note that in ALE methods the position of interfaces is a part of the solution and is not known in advance. For meshes not aligned with interfaces, we consider approaches in which the interfaces are not tracked explicitly, but reconstructed in multi-material cells, [28], by using interface reconstruction algorithms – [28,13,2]. The result of the interface reconstruction is shown in the right panel on Fig. 2. The input data for these interface reconstruction methods is the volumes of the materials in each cell of the base mesh and, optionally, some additional information, such as reference positions of centroids for all the materials inside MMCs. These methods reconstruct material interfaces in each cell of the base mesh in such a way that all the materials are represented by material polygons, where a given material polygon contains only one material, and the volume of that material is equal to the volume specified. This means that reconstructed material interfaces are piece-wise linear. The set of material polygons inside a multi-material cell forms a *minimesh*, see Fig. 3, left panel.

The most straightforward approach to solving diffusion problems on such meshes is by constructing a global polygonal mesh that is conformal to reconstructed interfaces, often called *supermesh*, Fig. 3, right panel, which has all pure single

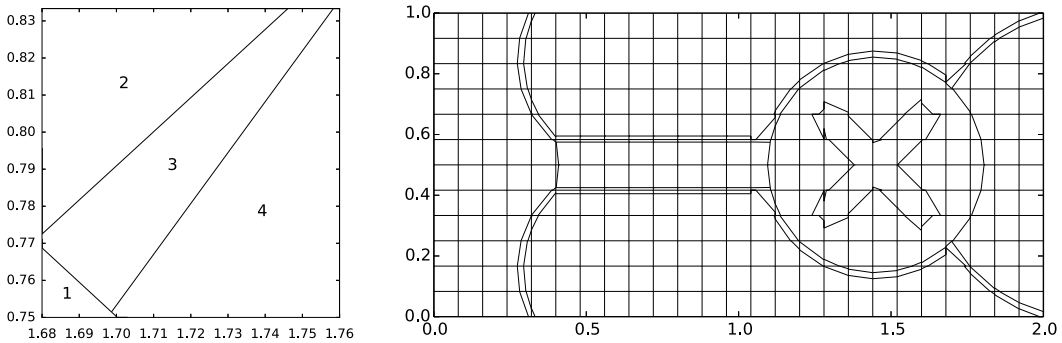

Fig. 3. Left – minimesh for cell 22, 10 of the base mesh (the center of this cell is approximately at $x = 1.75$, $y = 0.8$; right – supermesh: here, all the segments of material interfaces are faces of the supermesh.

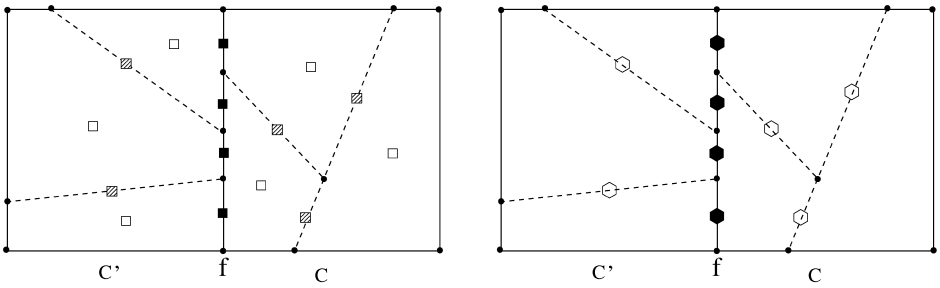

Fig. 4. Cells of the supermesh in two adjacent cells, C and C' of base mesh which share face f of supermesh. Left panel – temperature unknowns: empty squares are material temperatures, shaded squares are face temperatures on internal (with respect to base mesh) faces of the material polygons; solid black squares face temperatures on faces of the material polygons which coincide with pieces of the face f of base mesh. Right panel – flux unknowns: empty are hexagons are fluxes between materials inside cell of base mesh; solid black hexagons are fluxes between material polygons material polygons in cells C and C' of base mesh.

material polygons as cells [16]. The supermesh will be a general unstructured polygonal mesh even if the base mesh was a regular structured mesh. In Fig. 4 we show two adjacent cells of base mesh subdivided into material polygons, which are cells of the supermesh and related unknowns for supermesh approach. The construction of the supermesh requires establishing overall connectivity between material polygons (cells of minimeshes) in different cells of the base mesh. This is a non-trivial computational geometry problem, which, in general, makes this approach infeasible in 3D for general polyhedral meshes. Moreover, even in 2D this approach requires the use of the advanced discretization techniques on the supermesh, which are accurate on meshes with small edges and co-linear faces.

Another approach to solving diffusion equations on meshes with multi-material cells is to first use some kind of *homogenization*[1] of the material properties in multi-material cells, then solve the diffusion problem for unknowns associated with the base mesh. In such homogenization algorithms one typically assumes that each cell contains a single "homogenized" material, and its properties are calculated based on a volumetric distribution of different materials. The simplest homogenization approaches use harmonic and arithmetic averages. Let us note that those approaches have some meaning in the case of scalar conductivities on simple rectangular meshes or meshes where materials inside MMCs are distributed according to special patterns (e.g., forming vertical or horizontal strips), but we are not aware of any justification for the use of those approaches on general polygonal meshes or for general conductivity tensors. After the global problem on the base mesh which uses "homogenized" pure cells is solved, one obtains, say, one temperature per cell of the base mesh. At the final stage, one needs to decide how to determine material temperatures in each material of the multi-material cell from this single cell-averaged value and problem parameters. In our opinion those methods are ad-hoc, interested reader may read [10], in which some options are discussed. In Section 2 we show that homogenization methods can lead to qualitatively wrong results.

Known alternatives include possible use of mortar methods [15], which were developed in the context of dealing with non-matching meshes. This approach involves a delicate balancing of the mortar space and the traces of velocity spaces on the interface. The mathematical criteria for this balance are not constructive in general [1,26]. This makes the use of this approach on multi-material meshes with complex structures challenging. To the best of our knowledge, mortar types of methods have never been used to deal with multi-material cells.

[1] Let us note that this homogenization is not the same as the one used in classical homogenization theories related to periodic structures, [18].

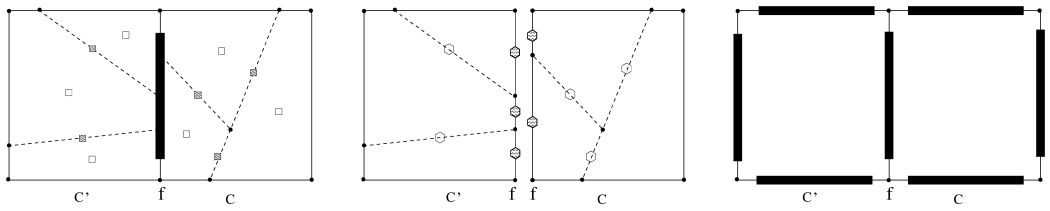

Fig. 5. Approximate static condensation. Left panel: all temperatures on the face f of base mesh are the same – marked by long black rectangle, the rest of notations is the same as in left panel in Fig. 4. Middle panel: exploded view of two adjacent cells of the base mesh; on common face f each cell has only their "own" fluxes marked by pentagons with wavy shading. Right panel – stencil for equation for face temperatures of the base on face f.

Recently, many papers on the Nitsche's method used in the framework of cut-cells or unfitted finite element methods considered the case of material interfaces non-aligned with a mesh, see for example, [17,9,3] and references therein. Another approach is to use the extended finite element methods (X-FEM) [12]. This group of methods was developed for a different type of problems, and most of those methods only deal with the two-materials case. Also, to the best of our knowledge, cut-cells methods assume continuous or almost continuous representation of interfaces between cells of the base mesh and can demonstrate a significant loss of accuracy as discontinuity grows [3], which is unavoidable in volume-of-fluid (VOF) interface reconstruction methods. Also, these methods are typically not locally conservative.

Main topic of this paper is a new method for solving diffusion equations on general polygonal meshes which contain MMCs. We call this method the *approximate static condensation (ASC)*. Here we will give just a brief description of the design principles of the new method, detailed description will be given in Section 4.2 and Appendix A.

The new method includes three main stages. The first stage is forming the matrix and the right-hand-side of the global system of equations. The global system is formulated with respect to temperatures on the faces of the base mesh – *one temperature per face*. To explain the main idea, we consider governing equations on a minimesh of a multi-material cell – *each cell of the base mesh considered separately*. We can discretize these equations first assuming that all temperatures on the one face of base mesh are the same and considering these temperatures on the faces of the base mesh as the Dirichlet boundary conditions for equations on minimesh inside cell of base mesh – Fig. 5. Let us note that notations in left panel in Fig. 5 are the same as in left panel in Fig. 4 with exception that now all temperatures on the face f are the same, which is emphasized by denoting it by long black rectangle. Clearly this is approximation. In the middle panel in Fig. 5 we present exploded view of two adjacent cells of the base mesh. Now on common face f each cell has only their "own" fluxes which correspond to intersection of faces of the material polygons in the cell with face f. If we use a conservative mixed-hybrid discretization, [8,25,23], then by inverting small matrices we can express all quantities in the multi-material cell in terms of face temperatures and consider them as parameters. In particular, we can express in this way the fluxes on the intersections of the boundary of the base cell with boundaries of the material polygons. For example, in the case presented in middle panel in Fig. 5 for cell C' we will have three one-sided fluxes on the face f and for cell C we have two one-sided fluxes on face f. Those fluxes will be expressed in terms of four face temperatures (which become new unknowns) in corresponding cells of the base mesh and known quantities such as conductivity coefficients, heat capacities, right-hand sides of the equations, and material temperatures on the previous time level.

The global system is formed by requiring the total flux from one side of a face of the base mesh to be equal to the total flux from the other side. This condition can be considered as enforcing some form of weak continuity of flux. The resulting global system will contain only temperatures on faces of the base mesh – for example presented in Fig. 5 stencil for equation corresponding to face f is shown in right panel of this figure and consist of seven face temperatures. The sparsity structure of the matrix in the global system does not change in comparison to the case where all cells are pure, and, in particular, it is the same as for homogenization methods. Clearly, elements of the matrix and the right-hand-side are different. We show that the matrix of this global system is symmetric and positive definite (SPD) in Appendix A. We call the described method the *approximate* static condensation – it is approximate because we assume that there is only one face temperature on the face of the base mesh, which is clearly an approximation.

One can attempt to interpret the ASC method as the coarsening procedure that follows the discretization of the considered problem using a conservative mixed hybrid scheme on a supermesh. The standard algebraic system on the supermesh can be condensed into a system in terms of temperatures on faces that belong to faces of the base mesh. Then, the approximate condensation can be performed by assuming that the temperature is constant on each face of the base mesh. Substituting unknowns on subfaces by a single degree of freedom and accumulating the respective equations, we obtain the system matrix of dimension equal to the number of faces in the base mesh, just as in the above description of the first stage. The important consideration is that the choice of stabilizing parameters used by the mimetic finite difference (MFD) methods depends on the geometry of a cell and in practice can be different for cells of minimeshes and cells of the supermesh: while the connectivity between geometrically adjacent cells of different minimeshes is not established, the topology of the supermesh includes the full connectivity information. In general, the supermesh can have more faces belonging to the same face of the base mesh than either of the minimeshes adjacent to that face. Therefore, a cell of the supermesh may have more faces, some of them possibly very small, than the corresponding cell of the minimesh, or the supermesh may

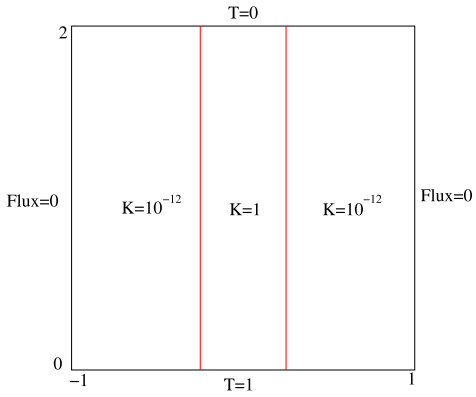

Fig. 6. Statement of the "sanity check" problem – planar sandwich.

contain additional highly anisotropic cells not present in any of the minimeshes, in which case the described procedure will result in a different algebraic system and potential loss of accuracy.

The second stage is solving the global system. The matrix of the global system is SPD and therefore some efficient iterative methods can be used. As the result, we obtain the face temperatures.

The final third stage is the backward substitution. In each cell of the base mesh we solve a local Dirichlet problem using the obtained face temperatures as the Dirichlet boundary conditions. These local problems can be solved independently of each other, giving us the temperatures for each material in the cell of the base mesh.

The paper is organized as follows. In Section 2, we present a very simple *sanity check* example and show that standard homogenization methods can lead to qualitatively wrong results, while the ASC method gives qualitatively correct results. The informal description of approximate static condensation is presented in Section 4.2. The formal description of the new method is given in Appendix A, where we also show that the matrix in the global algebraic system is symmetric and positive definite. The numerical examples which demonstrate performance of the new method are given in Section 5. In this section we also show the comparison with standard homogenizations methods described in Section 4.1. The conclusions and future work plans are described in Section 6.

2. Sanity check example

In this Section we present a very simple example, which we call "planar sandwich". This example is easy to reproduce. As the motivation for the rest of the paper, we show a qualitative comparison of the homogenization methods with the new ASC approach.

We solve equation (1) in the computational domain $(x, y) \in [-1:1] \times [0:2]$, Fig. 6, with boundary conditions $T = 1$ on $y = 0$; $T = 0$ on $y = 2$; $(K\nabla T) \cdot \mathbf{n} = 0$ on $x = -1$ and on $x = 1$ and initial conditions: $T|_{t=0} = 0$. We assume that $\rho c_p = 1$ and that the conductivity coefficient $\mathbf{K}$ is scalar, $\mathbf{K} = k\mathbf{I}$, where k is such that $k = 10^{-12}$, $x \in (-1, -0.25)$ and $x \in (0.25, 1)$; $k = 1$, $x \in (-0.25, 0.25)$; it is a two-material problem.

Reference solution for this problem can be obtained by using a fine logically rectangular mesh aligned with material interfaces. We present results for the time $t = 0.505$.

To discretize this problem we use the fully implicit discretization in time and the mimetic discretization in space [23]. In our numerical experiments we use a Voronoi mesh obtained by ShaPo software, [27]. Interface reconstruction is performed using the moment-of-fluid interface reconstruction method [13,2], which is exact for interfaces that are straight lines.

For homogenization methods we set the temperatures of materials to be equal to the cell-centered temperature obtained from solving the global system with "homogenized" pure cells. As we mentioned in the introduction, there are many other ad-hoc methods to define material temperatures based on cell-centered temperatures, but those methods are problem specific while we want to show an example that anyone can reproduce.

On Fig. 7 we present the results obtained in the FLAG code [6] by C. Malone. Left panel in this figure represent the reference solution obtained on a very fine mesh aligned with material interfaces. For testing the homogenization and ASC methods, we use a Voronoi mesh shown in three right panels, which has approximately 40×40 cells. One can see white thin straight lines which are the result of the interface reconstruction. These interfaces cross Voronoi cells in a very irregular way, which means that multi-material cells have all kind of distribution of volume fractions. Two middle panels represent the results obtained using the homogenization approach – AA stands for the arithmetic average, and HA stand for the harmonic average. Right panel shows the result for the ASC method. For the ASC method each material polygon has its own temperature and is therefore filled with the respective color.

Clearly both homogenization methods give qualitatively wrong results even in the "eyeball norm" – the arithmetic average allows heat to escape from the high conductivity stripe, and the harmonic average does the exact opposite – it narrows

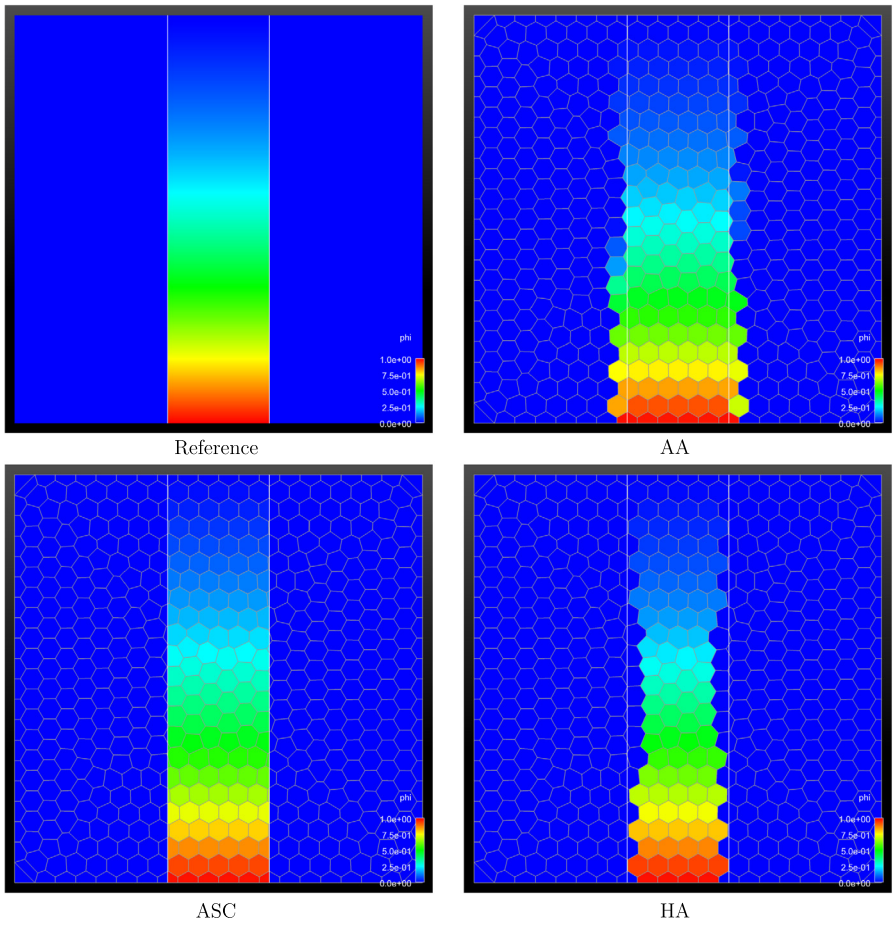

Fig. 7. Planar sandwich problem: Reference – reference solution, AA – homogenization with arithmetic average, HA – homogenization with harmonic average, ASC – approximate static condensation. (For interpretation of the references to color in this figure, the reader is referred to the web version of this article.)

the stripe through which the heat is flowing; in both cases it affects how much heat can flow through the domain. In Section 5 we will show more qualitative comparison results for the homogenization methods and the new ASC method.

Our conclusion from this simple example is that methods which are more accurate than the homogenization methods have to be developed.

3. X-MOF interface reconstruction method

The approximate static condensation approach requires the construction of a minimesh in each MMC along with a map between faces of material polygons and faces of the base mesh. In this section we briefly describe the eXtended Moment-of-Fluid (MOF) interface reconstruction method and the information about the minimesh that it creates.

The MOF method has been developed in [13,2] and since then has been used in many publications. It uses the volume fractions as well as the reference centroids as the input data for the interface reconstruction. Usually, interface reconstruction methods, including volume-of-fluid (VOF) and MOF, produce material polygons inside multi-material cells, but do not produce any connectivity information for those material polygons. For advanced closure models for hydrodynamics, [4], one may need information about face neighbors inside a multi-material cell. Usually this information is recovered on a separate step by analyzing boundaries of the material polygons. In general, this analysis uses some tolerances to decide if two lines do coincide or not, and so on – this is not a very robust procedure. In our case, we also need only the face connectivity information on a minimesh, and we also need to know which pieces of the boundaries of material polygons are parts of what faces of the cell of the base mesh.

We have created a new *eXtended Moment of Fluid – X-MOF* algorithm in which the full connectivity on a minimesh is established in the process of constructing the material polygons. This approach allows to avoid geometrically ambiguous situations.

In Fig. 8 we show the result of the interface reconstruction on the base mesh for the entire domain (left panel) and for cell $(5, 5)$ (right panel), which contains four different materials. In Fig. 9 we present the connectivity information for this cell.

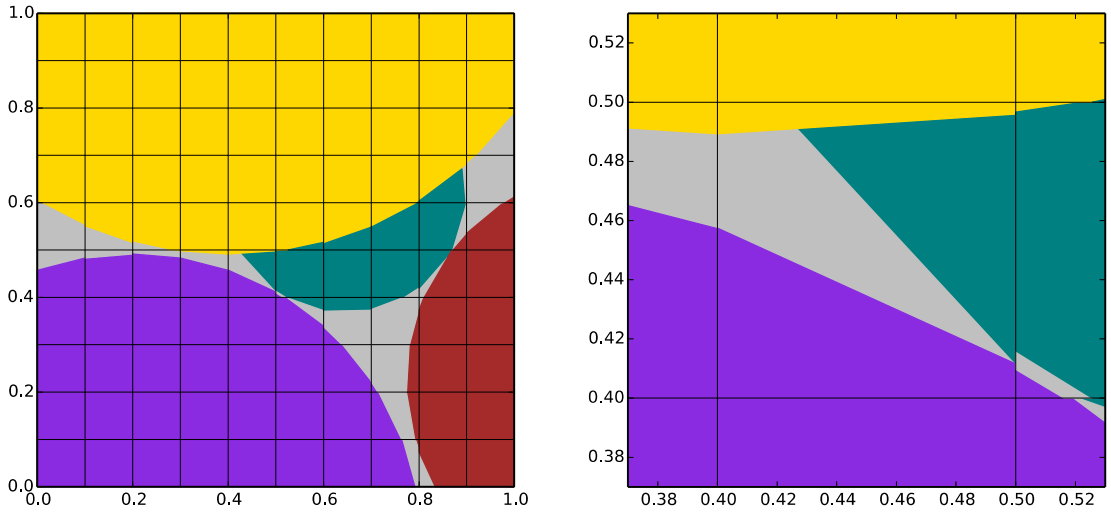

Fig. 8. Interface reconstruction on a base mesh – (left panel) entire domain, (right panel) cell (5, 5).

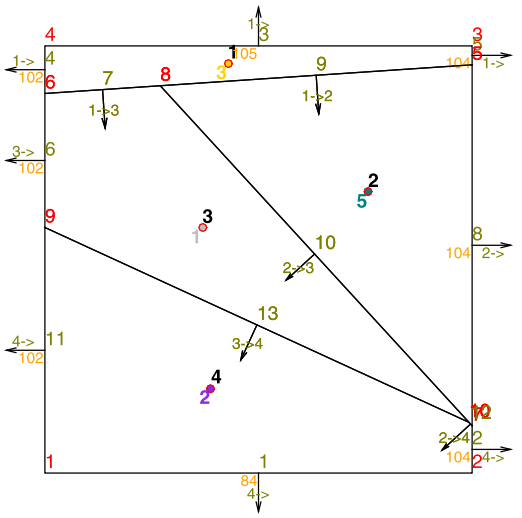

Fig. 9. Internal connectivity in cell (5, 5) and connection to faces of the base mesh. For subcells (material polygons) we show: subcell's index (black); global material index (in material's color – correspond to colors in Fig. 8; local nodes indices in the minimesh (red); local faces indices in the minimesh (olive). For subfaces we show: adjacent cell local indices with the directions of normals (olive); global indices of "parent" faces (orange). (For interpretation of the colors in this figure, the reader is referred to the web version of this article.)

The X-MOF algorithm gives the full connectivity information (see, Fig. 9): on the minimesh level, cells store IDs of their faces and nodes, faces store IDs of their nodes and adjacent cells along with directions of normals (for boundary faces normals are always directed outwards); between mesh levels local cells store global IDs of their materials and of their "parent" cells, faces store IDs of their "parent" faces in the base mesh, if any. This information is needed for the implementation of ASC.

4. Discretization methods

We use the backward Euler method to discretize problem (1) in time:

$$-\nabla \cdot (\mathbf{K} \nabla T^{n+1}) + \sigma T^{n+1} = f + \sigma T^{n}\,, \tag{3}$$

where $\sigma = \dfrac{\rho\, c_p}{\Delta t}$ and both ρ and c_p are assumed to be time-independent parameters. In the following subsections, we discuss methods to discretize problem (3) in space.

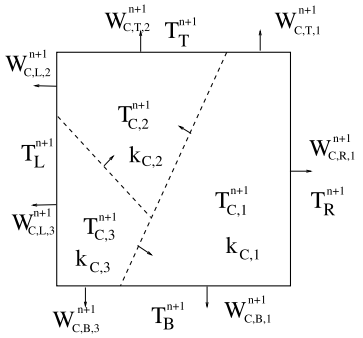

Fig. 10. Minimesh: notations.

4.1. Homogenization methods

The simplest homogenization method consists of three stages.

The first stage is the homogenization of conductivity coefficients and other material properties, that is, creating "pure" cell with averaged properties. Here we consider only the homogenization of conductivity coefficients: new values for the source function and other material properties are obtained by taking their volume-averages over material polygons. Homogenization requires only knowing the volume fractions, $\alpha_{C,m}$, of materials m in cell C. This information comes from the interface reconstruction. Arithmetic average is defined as follows:

$$k_C^A = \sum_{m \in M(C)} \alpha_{C,m} k_{C,m}\,, \tag{4}$$

where $M(C)$ is the set of all materials in the cell C, and $k_{C,m}$ is the conductivity for material m. Harmonic average is

$$k_C^H = (\sum_{m \in M(C)} \alpha_{C,m}/k_{C,m})^{-1}\,. \tag{5}$$

The second stage is the solution of global system of equations on the base mesh. It produces just one temperature for cell C at new time level: T_C^{n+1}.

The third stage is the recovery of material temperatures, $T_{C,m}^{n+1}$, for each material in the multi-material cell from T_C^{n+1}. This stage is often ad hoc. In our implementation used in Section 5, we set all material temperatures equal to T_C^{n+1}.

4.2. Approximate static condensation

As we have mentioned in the introduction, the ASC method includes three main stages.

The first stage is forming the global system. Consider a minimesh shown on Fig. 10. In this case a multi-material cell, C, consists of three materials with corresponding material polygons denoted by $C,1$; $C,2$ and $C,3$. These notations are used as subscripts for all quantities in Fig. 10. The superscript $n+1$ is used for unknown quantities at the new time level. Subscripts B, R, T, L are used as local IDs for the bottom, right, top and left faces of the base mesh. The temperatures on the faces of the base mesh (one per face) have those IDs as subscripts. Fluxes are denoted by w, in Fig. 10 we show only *external* fluxes, that is the fluxes on pieces of the faces of the base mesh which overlap with faces of the material polygons. Those "one-sided" fluxes inherit indices of the parent cell of the base mesh, the index of the face of the base mesh and the index of the material polygon inside the parent cell of the base mesh.

Consider a diffusion equation on a minimesh which consists of pure material polygons as a local Dirichlet problem with given temperatures (one per face of the base mesh). Then if we consider those face temperatures as unknown parameters, then by discretizing the problem on the minimesh and then inverting small local matrices, we can express all quantities inside the multi-material cell, including *one-sided* fluxes on the faces of the base mesh, in terms of the base face temperatures.

To form the global system with respect to the base face temperatures, we require the total flux from one side of the face of the base mesh to be the same to the total flux from another side

$$\sum_{m \in M(C)} w_{C,f,m}^{n+1} S_{C,f,m} = \sum_{m \in M(C')} w_{C',f,m}^{n+1} S_{C',f,m} \tag{6}$$

where f is the face of the base mesh common for cells C and C', S with subscripts are areas of corresponding parts of the face of the base mesh which are marked by different colors only, – see Fig. 11.

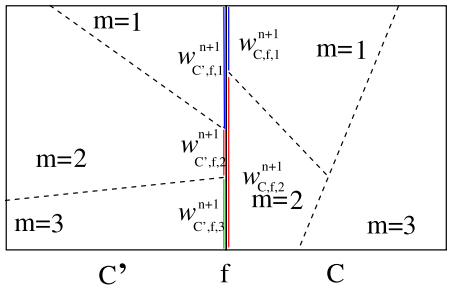

Fig. 11. Weak continuity of flux on interfaces of the base mesh.

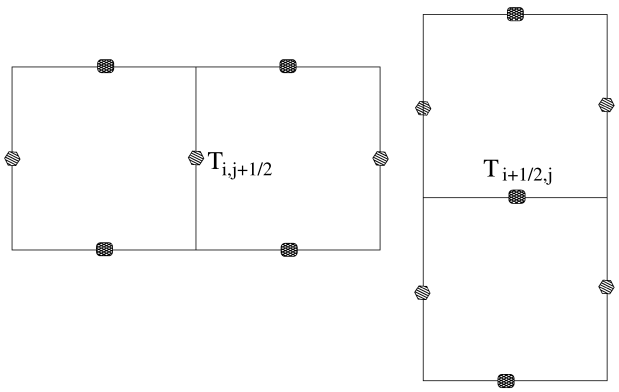

Fig. 12. Stencils for global system with respect to the face temperatures – logically rectangular mesh.

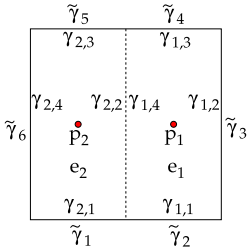

Fig. 13. A square multi-material cell.

On a logically rectangular mesh the stencil for resulting system is shown in Fig. 12. In Appendix A we show that the matrix in the resulting global system is symmetric positive definite (SPD).

The second stage is solving the global system of equations for temperatures on the faces of the base mesh. Because this system has an SPD matrix, many efficient iterative methods can be used.

The third stage is the backward substitution, that is solving local systems on minimeshes for given base mesh face temperatures, which are the result of the global solve – see Fig. 10. The local systems can be solved independently for each cell of the base mesh. Actually, it is not really solving the linear systems, but applying some small local matrices which were used in assembly of the global matrix to the vector of face unknowns. The result of the backward substitution is all material temperatures at t^{n+1}, and any other quantities related to the multi-material cell, if needed.

4.3. Simple example

Let us consider a simple example with a multi-material cell shown on Fig. 13: there, E is a square $h \times h$ cell with a minimesh E_h consisting of two rectangular material polygons e_1 and e_2 of equal size. Faces of cell e_i are denoted by $\gamma_{i,j}$, $i = 1, 2$, $j = \overline{1,4}$. Boundary faces in E_h are denoted by $\widetilde{\gamma}_j$, $j = \overline{1,6}$. Cell E has four "base" faces Γ_s, where $\Gamma_2 = \widetilde{\gamma}_3$, $\Gamma_4 = \widetilde{\gamma}_6$, and faces Γ_1, Γ_3 have two subfaces each: $\Gamma_1 = \widetilde{\gamma}_1 \cup \widetilde{\gamma}_2$ and $\Gamma_3 = \widetilde{\gamma}_4 \cup \widetilde{\gamma}_5$. It follows that $|\widetilde{\gamma}_1| = |\widetilde{\gamma}_2| = |\widetilde{\gamma}_4| = |\widetilde{\gamma}_5| = \frac{h}{2}$ and $|\widetilde{\gamma}_3| = |\widetilde{\gamma}_6| = |\gamma_{1,4}| = |\gamma_{2,2}| = h$. Let the diffusion coefficient be scalar and equal to k_i in e_i, $i = 1, 2$. We then denote their harmonic mean by k_H and their arithmetic mean by k_A:

$$k_H = \frac{2k_1k_2}{k_1+k_2}, \quad k_A = \frac{1}{2}(k_1+k_2). \tag{7}$$

Below we show the numerical fluxes on faces of E_h for discretizations described in Sections 4.1 and 4.2. The respective local matrices for this example are given in Appendix B.

4.3.1. Homogenization methods

In the case of homogenization methods, we discretize the problem on the base cell E using the averaged parameters values. Let us denote the diffusion coefficient by k_*, where $k_* = k_H$ or $k_* = k_A$ for harmonic and arithmetic means respectively.

We denote the cell-average value of the solution by p_c and use the mimetic finite differences to obtain the local algebraic system on the cell E. From the resulting expressions for numerical fluxes on faces of E which are denoted by $\widehat{w}_i$, $i = \overline{1,4}$, and setting $w_1 = \widehat{w}_1 = w_2$, $w_3 = \widehat{w}_2$, $w_4 = \widehat{w}_3 = w_5$, $w_6 = \widehat{w}_3$ we get

$$\begin{aligned} w_1 &= w_2 = -k_*\frac{\widehat{\lambda}_1 - p_c}{h/2}, \quad w_3 = -k_*\frac{\widehat{\lambda}_2 - p_c}{h/2}, \\ w_4 &= w_5 = -k_*\frac{\widehat{\lambda}_3 - p_c}{h/2}, \quad w_6 = -k_*\frac{\widehat{\lambda}_4 - p_c}{h/2}. \end{aligned} \tag{8}$$

4.3.2. ASC method

We use mimetic finite differences to discretize the problem on material polygons in E_h, and following the description of the ASC method in Section 4.2 we introduce temperatures on faces Γ_s and denote them $\widehat{\lambda}_s$, $s = \overline{1,4}$. Then we assume that $\widetilde{\lambda}_1 = \widehat{\lambda}_1 = \widetilde{\lambda}_2$, $\widetilde{\lambda}_3 = \widehat{\lambda}_2$, $\widetilde{\lambda}_4 = \widehat{\lambda}_3 = \widetilde{\lambda}_5$, and $\widetilde{\lambda}_6 = \widehat{\lambda}_4$ where $\widetilde{\lambda}_j$ are temperatures on faces $\widetilde{\gamma}_j$ of the minimesh E_h.

Let w_i be the numerical fluxes on faces γ_i, then it can be derived that

$$\begin{aligned} w_1 &= -k_2\frac{\widehat{\lambda}_1 - p_2}{h/2}, \quad w_2 = -k_1\frac{\widehat{\lambda}_1 - p_1}{h/2}, \\ w_3 &= -k_1\frac{\widehat{\lambda}_2 - p_1}{h/4}, \quad w_4 = -k_1\frac{\widehat{\lambda}_3 - p_1}{h/2}, \quad w_5 = -k_2\frac{\widehat{\lambda}_3 - p_2}{h/2}, \\ w_6 &= -k_2\frac{\widehat{\lambda}_4 - p_2}{h/4}, \quad w_{1,2} = -k_H\frac{p_2 - p_1}{h/2}, \end{aligned} \tag{9}$$

where $w_{1,2}$ is the numerical flux on the interface between subcells e_1 and e_2 with the normal directed from e_1 to e_2.

4.3.3. Limiting case

Let us assume that E is a high-contrast multimaterial cell. We set $k_1 = 1$ and $k_2 \to 0$, then $k_H \to 0$ and $k_A \to \frac{1}{2}k_1$.

For the homogenization method with the harmonic mean we then have

$$\begin{aligned} w_1 &= w_2 \to 0, \quad w_3 \to 0, \\ w_4 &= w_5 \to 0, \quad w_6 \to 0, \end{aligned} \tag{10}$$

which means that there is no flow through cell E.

For the homogenization method with the arithmetic mean we have

$$\begin{aligned} w_1 &= w_2 = -k_1\frac{\widehat{\lambda}_1 - p_c}{h}, \quad w_3 = -k_1\frac{\widehat{\lambda}_2 - p_c}{h}, \\ w_4 &= w_5 = -k_1\frac{\widehat{\lambda}_3 - p_c}{h}, \quad w_6 = -k_1\frac{\widehat{\lambda}_4 - p_c}{h}, \end{aligned} \tag{11}$$

which implies that the vertical component of flow through subcells e_1 and e_2 is the same.

For the ASC method we obtain

$$\begin{aligned} w_1 &\to 0, \quad w_2 = -k_1\frac{\widehat{\lambda}_1 - p_1}{h/2}, \quad w_3 = -k_1\frac{\widehat{\lambda}_2 - p_1}{h/4}, \\ w_4 &= -k_1\frac{\widehat{\lambda}_3 - p_1}{h/2}, \quad w_5 \to 0, \quad w_6 \to 0, \quad w_{1,2} \to 0, \end{aligned} \tag{12}$$

which means that there is no flow through e_2, and the flow through e_1 is bigger than the one that the homogenization method with the arithmetic mean provides.

We can conclude that only the ASC method is able to resolve the limiting case correctly.

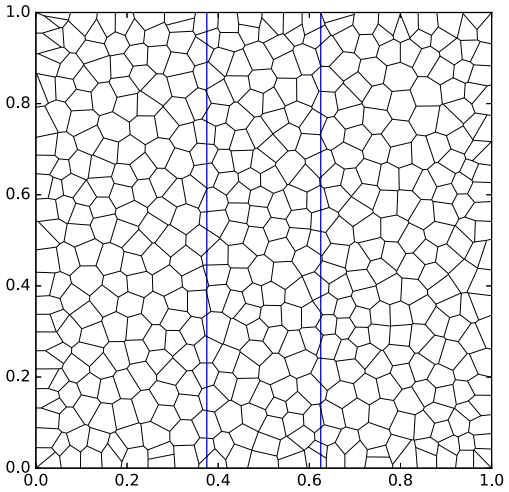

Fig. 14. Three material planar sandwich.

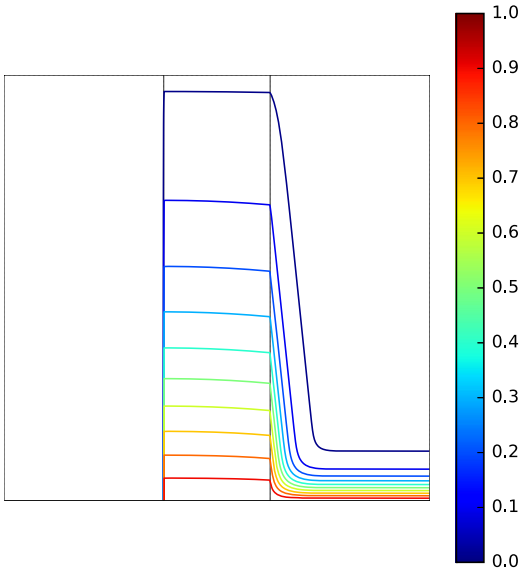

Fig. 15. Three material planar sandwich – reference solution, contour lines.

5. Numerical examples

Here, we present several numerical examples which demonstrate the performance of the ASC method. In Section 5.1, we consider an example which is similar to the planar sandwich example presented in Section 2, but with three different materials. We give quantitative comparison of the new ASC method and the homogenization approach, as described in 4.1. In Section 5.2 we present results for the flow in a sand and shale system and, again, give quantitative comparison of new ASC method and the homogenization approach. Examples in Sections 5.1 and 5.2 deal with discontinuous scalar conductivity coefficient. In Section 5.3 we consider flow through the system with a low-permeability streak in which permeability is a full tensor. For this problem we present only the ASC results because we are not aware of homogenization methods for the case when coefficients are tensorial. Other numeral examples can be found in [20,11].

5.1. Modified planar sandwich

In this section we will consider modified version of the planar sandwich problem, Fig. 14. The current problem is posed on a unit square with the stripe from $x = 0.375$ to $x = 0.625$. The final time is 0.1 and the time step is 10^{-3}, but now we consider the case of three materials – the diffusion coefficient in the left part of the domain is 10^{-12}, in the middle it is 1, and in the right part it is 10^{-2}. The boundary conditions are as follows – no flux on the left and right boundary, temperature is equal to 1 on the bottom boundary and zero on the top boundary.

The reference solution has been obtained using a conforming mesh with 512×512 cells and it is shown in Fig. 15.

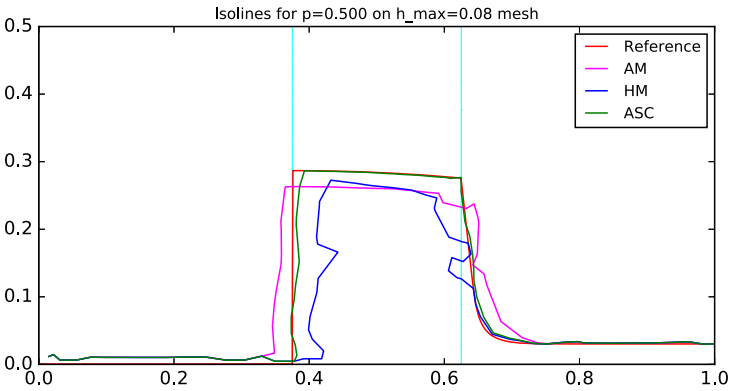

Fig. 16. Three material planar sandwich – contour lines for temperature $T = 0.5$ and $h_{max} = 0.08$. Reference – reference solution, ASC – approximate static condensation, HM – harmonic homogenization, AM – arithmetic homogenization.

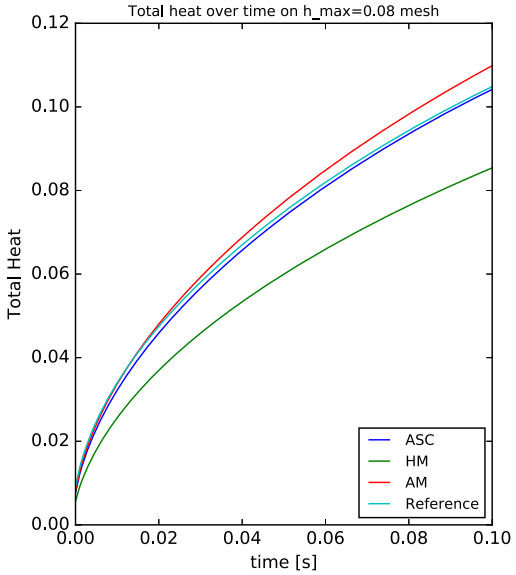

Fig. 17. Three material planar sandwich – dynamics of the total heat in the system for $h_{max} = 0.08$.

Table 1
Modified planar sandwich. The discrete L_2 error.

Method	$h_{max} = 0.08$	$h_{max} = 0.04$	$h_{max} = 0.02$	$h_{max} = 0.01$
ASC	0.00618	0.00501	0.00316	0.00187
HM	0.07979	0.04887	0.03937	0.02725
AM	0.07017	0.05868	0.04235	0.02937

We present results for the series of Voronoi meshes generated with ShaPo software [27]. We use ConVorM option in this software, which require us to specify the characteristic mesh size. We use $h_{max} = 0.08, 0.04, 0.02, 0.01$, which produces meshes with $465, 1770, 6903, 27387$ cells respectively. The mesh for $h = 0.08$ shown in Fig. 14.

In Fig. 16 we show the contour lines for all methods for temperature $T = 0.5$ and $h_{max} = 0.08$. In Fig. 17 we show the dynamics of the total heat in the system, $(\sum_i T_i |e_i|$, where the sum is over all material polygons e_i, T_i is the temperature in the material polygon, and $|e_i|$ is its area. The values of total heat at the final time moment are: Reference – 0.10484, ASC – 0.10417, HM – 0.08540, and AM – 0.10985.

The qualitative conclusions from those graphs are the same as quantitative conclusions in the "sanity check" planar sandwich problem in Section 2. That is, the ASC method is the most accurate one for this problem, AM approach allows heat to spread too much outside the stripe and produces too much total heat, but the heat front is moving slower than it should; for HM the heat is concentrated in a more narrow stripe, and the total flux is much lower than it has to be.

The discrete L_2 errors for the three methods with respect to the reference solution are presented in Table 1. The errors in material polygons e_i are computed by finding the closest cell in the reference mesh and comparing those two numbers

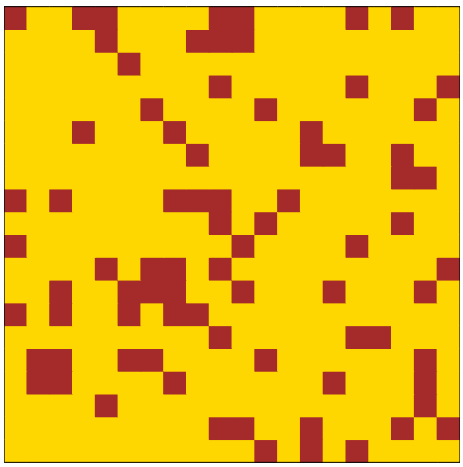

Fig. 18. Subdomains structure: sand is in gold, shale is in brown. (For interpretation of the colors in this figure, the reader is referred to the web version of this article.)

– $T_i - T_i^{ref}$. Then the discrete L_2 norm of this difference is $\left(\sum_i \left(T_i - T_i^{ref}\right)^2 |e_i|\right)^{1/2}$). Let us note that for the reference solution the discrete L_2 norm over the reference mesh was 0.24527. For all the resolutions the error for ASC method is about ten times lower than one for the HA and AM methods. However, it appears that all methods converge in this norm.

5.2. Sand and shale

This example is taken from [14] and was used in many papers, for example, see [19]. To be consistent with the original paper, we will call the scalar unknown pressure, call the flux velocity, and call the conductivity coefficient permeability. The computational domain is a unit square. Pressure is equal to one along $x = 0$, and to zero along $x = 1$. Flux is equal to zero along $y = 0$ and $y = 1$. The permeability field is generated by randomly placing shales with the total area fraction 0.2 throughout the sand. This is done on a regular grid with dimensions 20×20. The domain Ω with subdomains colored by the type of the material is shown on Fig. 18. In the example, the permeabilities of both the sand, (k_{sand}), and the shale, (k_{shale}), are taken to be uniform and isotropic, $\mathbf{K} = \mathrm{k}\mathbf{I}$, with $\mathrm{k}_{sand} = 1$ and $\mathrm{k}_{shale} = 10^{-6}$. We solve the stationary diffusion problem and are primarily interested in the total flux through the system. In the original article, the total flux through the system was obtained by using the standard, five-point finite volume method on a sequence of meshes aligned with material interfaces, with the finest mesh being 200×200, which gives total the flux of 0.5205. To obtain the reference solution, we solve the problem on a 400×400 mesh aligned with material interfaces by using a method from [21,22]. The result obtained in this way is 0.519269, which we will consider as the reference value for the total flux. In this section we present results on the same sequence of Voronoi meshes as in the previous section. We would like to demonstrate that numerical results depend both on the accuracy of the interface reconstruction and the approach used for dealing with multi-material cells. In Fig. 19 we present results of interface reconstruction for two mesh resolutions: $h_{max} = 0.08$ and $h_{max} = 0.04$ Clearly, interfaces are much more accurate for finer mesh. In Table 2 we present total flux on non-aligned Voronoi mesh for different spatial resolution. One can see that the ASC method is the least sensitive to resolution and therefore to the accuracy of the interface reconstruction. For all resolutions ASC gives the most accurate results. The most dramatic difference is observed for lower resolution. The main conclusion from this table is that ASC can be used on low resolution meshes and produce reasonable results.

In Table 3 we present the discrete L_2 errors in pressure with respect to the reference solution. It is interesting to observe that on lower resolution meshes ASC is more accurate, however, on the highest resolution mesh the harmonic homogenization gives more accurate results in this norm. Also, it appears that for this problem the ASC method converges slower than the harmonic homogenization or maybe does not converge at all. We have the following explanation for this phenomenon. The ASC method was created under the assumption that there are distinct interface between different materials. The sand and shale problem is a problem which models a random distribution of the shale in the sand, thus there are no distinct interfaces and the homogenization approaches may lead to better local accuracy.

Another thing no note is a significant jump in errors between $h_{max} = 0.04$ and $h_{max} = 0.02$ meshes. This is a good illustration of an impact that interface reconstruction can have on the overall accuracy: on Fig. 20, we show reconstructed interfaces along with the reference ones for both resolutions. It can be seen that refining the mesh also results in structural changes, where subdomains containing the same material can join or split. This effect can be clearly observed in the central part of the domain, say, around the coordinates $(0.5, 0.4)$ and $(0.45, 0.3)$. This change has a contribution on the same order of magnitude as decreasing the cells' size does, and can become even more critical depending on the distribution of material in a domain.

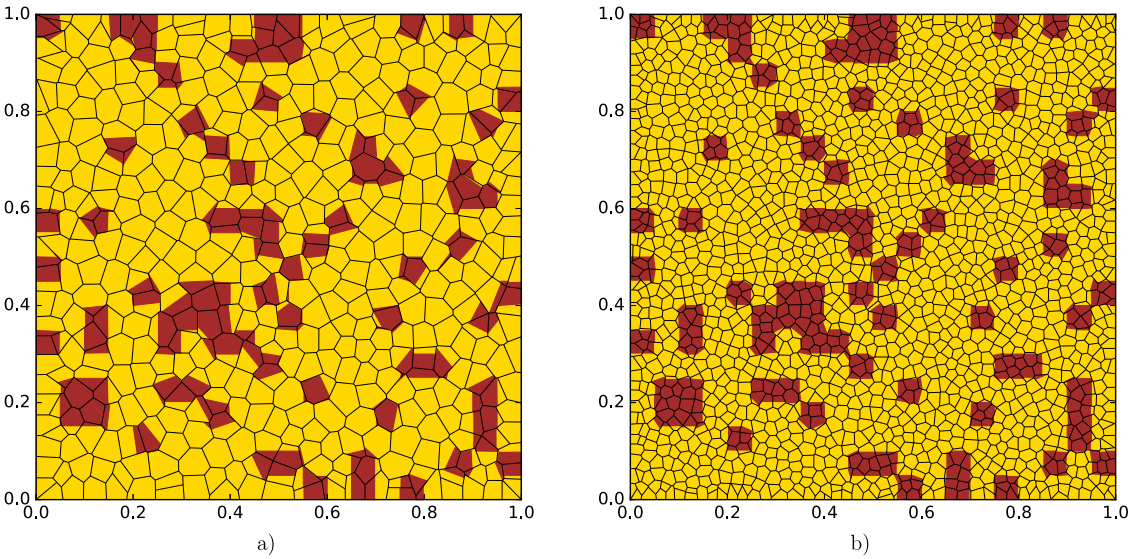

Fig. 19. Sand and shale problem. Interface reconstruction on Voronoi mesh: a) – $h_{max} = 0.08$; b) $h_{max} = 0.04$.

Table 2
Sand and shale problem. Total flux through the system for meshes non-aligned with material interfaces.

Method	$h_{max} = 0.08$	$h_{max} = 0.04$	$h_{max} = 0.02$	$h_{max} = 0.01$
ASC	0.525587	0.568679	0.560222	0.561952
HM	9.4055e-05	0.194319	0.395264	0.456251
AM	0.704751	0.637985	0.601366	0.589763

Table 3
Sand and shale problem. The discrete L_2-error in T for meshes non-aligned with material interfaces ($\|T\|_{L_2} = 0.593361963$ for the 400×400 aligned mesh).

Method	$h_{max} = 0.08$	$h_{max} = 0.04$	$h_{max} = 0.02$	$h_{max} = 0.01$
–ASC	0.02578363	0.02530945	0.02012568	0.01837084
HM	0.16676408	0.08541107	0.01299895	0.00617034
AM	0.04280296	0.03687728	0.0304548	0.02824728

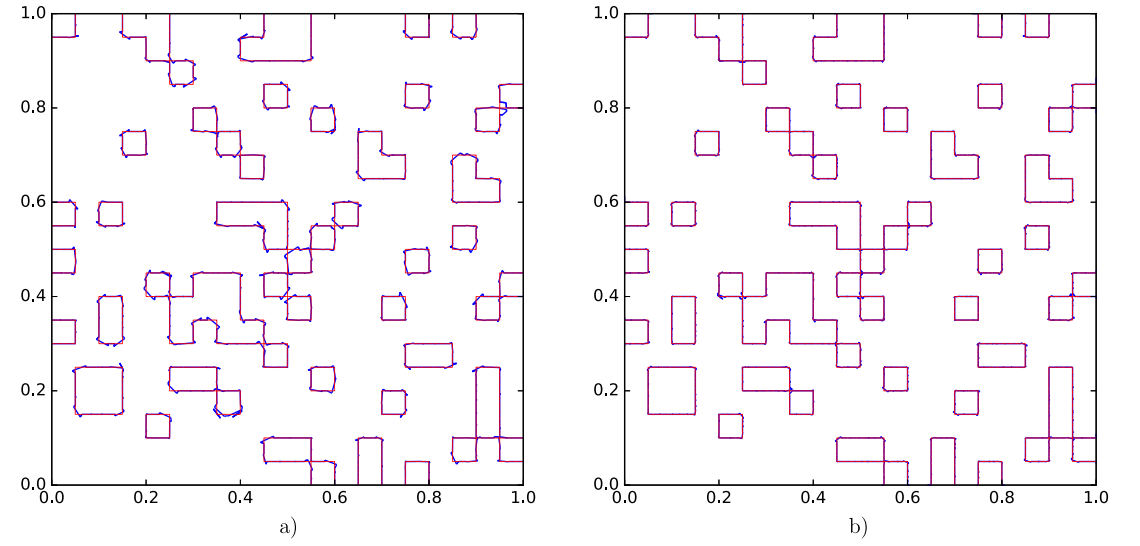

Fig. 20. Sand and shale problem. Material interfaces on Voronoi mesh: a) – $h_{max} = 0.04$; b) $h_{max} = 0.02$.

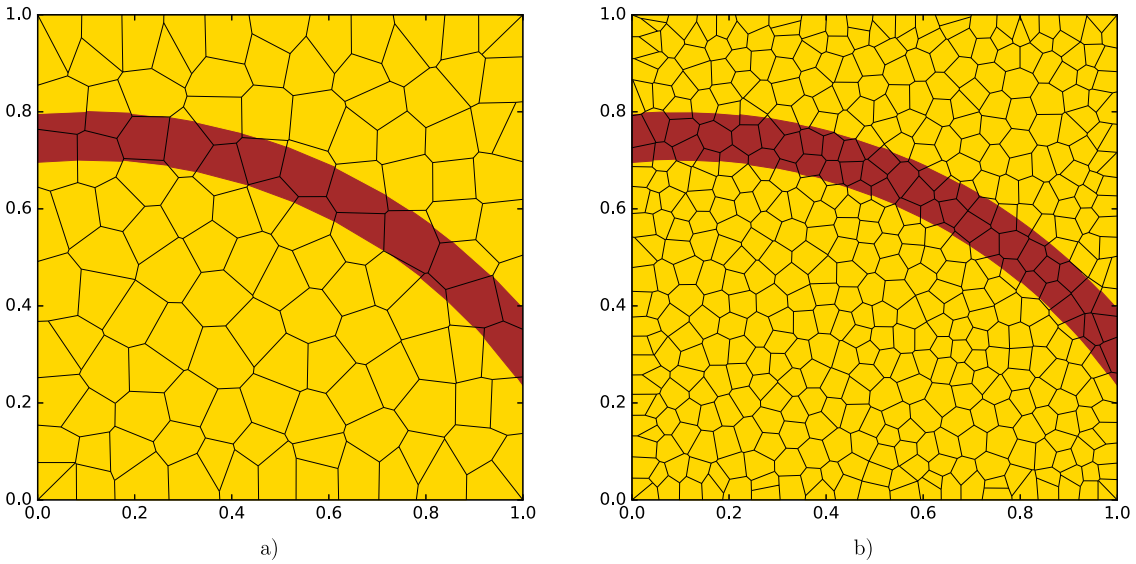

Fig. 21. Low-permeability streak – geometry and mesh: a) $h_{max} = 0.16$, b) $h_{max} = 0.08$.

5.3. Low-permeability streak

This problem, the geometry for which is shown on Fig. 21, is also taken from [14]. The top curve is a part of the circle with the center at the point $(0.1, -0.4)$ and the radius equal to 1.2. The bottom curve is also a part of the circle with the same center and with the radius equal to 1.1. The permeability throughout the domain is uniform and isotropic ($\mathbf{K} = \mathbf{I}$), except in the low-permeability streak shown in Fig. 21, where the permeability is set such that the component parallel to the local streak orientation ($\mathrm{k}_{\parallel}$) is equal to 0.1, and the component perpendicular to the streak orientation ($\mathrm{k}_{\perp}$) is equal to 0.001. The tensor $\mathbf{K}$ in the streak is a full tensor in terms of its Cartesian components, which vary with (x, y) and are readily determined from the knowledge of $\mathrm{k}_{\parallel}$ and $\mathrm{k}_{\perp}$. For the Cartesian components $\mathbf{K}_{xx}, \mathbf{K}_{xy}, \mathbf{K}_{yy}$, which are used in the code, the transformation formulas are:

$$K_{xx} = \mathrm{k}_{\parallel} \cos^2\varphi + \mathrm{k}_{\perp} \sin^2\varphi\,, \tag{13}$$

$$K_{xy} = (\mathrm{k}_{\parallel} - \mathrm{k}_{\perp}) \cos\varphi \sin\varphi\,, \tag{14}$$

$$K_{yy} = \mathrm{k}_{\parallel} \sin^2\varphi + \mathrm{k}_{\perp} \cos^2\varphi\,, \tag{15}$$

where $\varphi = \varphi(x, y)$ is the angle of rotation of the orthogonal coordinate system where the tensor $\mathbf{K}$ is diagonal and has components $\mathrm{k}_{\parallel}$ and $\mathrm{k}_{\perp}$. In our case

$$\sin\varphi = -\frac{\widetilde{x}}{\sqrt{(\widetilde{x})^2 + (\widetilde{y})^2}}\,, \tag{16}$$

$$\cos\varphi = \frac{\widetilde{y}}{\sqrt{(\widetilde{x})^2 + (\widetilde{y})^2}}\,, \tag{17}$$

where $\widetilde{x} = x - 0.1$ and $\widetilde{y} = y + 0.4$.

The boundary conditions for this problem are the same as in the previous section – no flux on the top and bottom, the pressure of one on the left boundary and of zero on the right boundary.

For this problem we present only results for our new ASC method because it is not clear how to perform the homogenization of tensorial coefficients.

As one can see from Fig. 21, the interface reconstruction is very accurate for this problem because interfaces are smooth. For the lowest resolution there is at least one cell (around $(x, y) = (0.3, 0.75)$) which is subdivided into three pieces, there are also cells with very small parts of the streak in them.

In Table 4 we show the total flux through the system. The reference total flux obtained on the high resolution interfaces-aligned mesh is equal to 0.7565. As in the previous problem, we can see that the ASC method is relatively accurate and does not require mesh refinement to obtain a satisfactory value of this integral characteristic.

In Fig. 22, for two resolutions we present the velocity field obtained from the reference solution and from the ASC solution. We can see that for the lowest resolution there is some discrepancy with the reference solution in cells which are close to multi-material cell containing three materials, as well as near the right boundary around the streak. On the finer meshes those artifacts are not present. We are planning to investigate this behavior in the future papers.

Table 4
Low-permeability streak. Total flux through the system for meshes non-aligned with material interfaces.

$h_{max} = 0.16$	$h_{max} = 0.08$	$h_{max} = 0.04$	$h_{max} = 0.02$	$h_{max} = 0.01$
0.7590	0.7569	0.7566	0.7568	0.7570

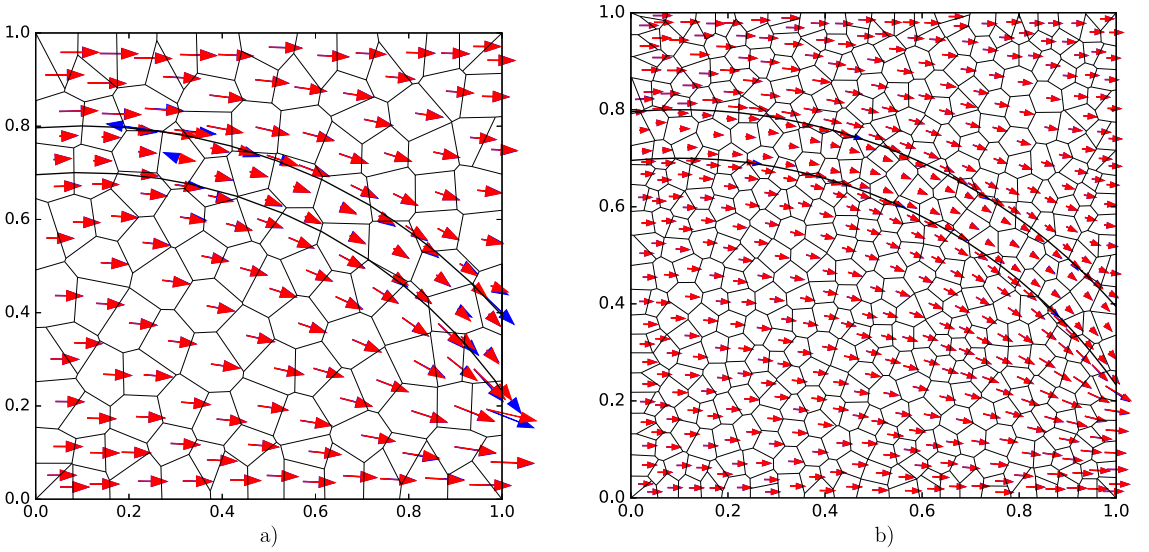

Fig. 22. Low-permeability streak – velocity field, red arrows are for reference solution, blue arrows are for ASC solution: a) $h_{max} = 0.16$, b) $h_{max} = 0.08$. (For interpretation of the colors in this figure, the reader is referred to the web version of this article.)

Table 5
Low-permeability streak. Discrete L_2 error in pressure ($\|p\|_{L_2} = 0.617162826$ for the 500×500 aligned mesh).

$h_{max} = 0.16$	$h_{max} = 0.08$	$h_{max} = 0.04$	$h_{max} = 0.02$	$h_{max} = 0.01$
0.0166	0.0173	0.0093	0.0040	0.0024

The discrete L_2 error with respect to the reference solution is presented in Table 5. In contrast with the sand and shale problem, this problem has distinct interfaces between materials and from Table 5 we can observe the first-order convergence rate.

6. Conclusions and future work

In this paper we have introduced new approximate static condensation (ASC) method for solving multi-material diffusion equations with discontinuous tensorial coefficients on general unstructured polygonal meshes non-aligned with material interfaces. The ASC method consists of three stages. At the first stage we build the global system of equations with respect to the temperatures on faces of the base mesh (one temperature per face). This system is obtained by first using the approximate static condensation to eliminate all internal unknowns inside multi-material cell, and then enforcing the weak flux continuity on faces of the base mesh. The global system with respect to face temperatures is symmetric and positive definite, and has the same sparsity structure as in the case of the mesh with only pure cells.

We have demonstrated that for problems with distinct material interfaces the ASC method is more accurate than traditional homogenization methods. Also we have shown that the ASC method works for the case of tensorial coefficients when it is not clear how to use the homogenization methods.

Clearly, the ASC method has its own deficiencies, which result from the assumption that we have only one temperature on the face of the base mesh. However, the numerical results presented in the current paper and in [20,11] show that the ASC methods gives plausible results for a wide range of problems.

As such, it is clear that further improvements of the ASC type of algorithms has to be developed in order to cover the wider range of real-life applications. One direction is to enrich the spaces used to approximate the solution on the interfaces between the multi-material cells. Alternatively, we can still use only one degree of freedom per face of the base mesh, but modify the local approximation procedure to better capture the geometry of minimeshes and use the information from the previous time step and from the neighboring cells. This will be addressed in future papers.

Acknowledgements

This work was performed under the auspices of the National Nuclear Security Administration of the US Department of Energy at Los Alamos National Laboratory under Contract No. DE-AC52-06NA25396. The authors gratefully acknowledge the partial support of the US Department of Energy Office of Science Advanced Scientific Computing Research (ASCR) Program in Applied Mathematics Research and the partial support of the US Department of Energy National Nuclear Security Administration Advanced Simulation and Computing (ASC) Program. LA-UR-17-22479.

The authors thank A. Dawes, C. Malone, D. Burton, D. Svyatsky, J. Fung, T.Masser, W. Dai, M. François, D. Kuzmin, G. Manzini, J. Morel, and J. Dolbow for many useful discussions.

Appendix A. Formal description of the ASC method

Let Ω be a polygonal domain and let $\boldsymbol{w} = -\mathbf{K}\nabla T$ be the flux vector function. We consider the following diffusion problem written in the mixed form:

$$\begin{aligned} \mathbf{K}^{-1}\boldsymbol{w} + \quad \nabla T &= 0 \quad \text{in } \Omega\,, \\ \nabla\cdot\boldsymbol{w} + \quad \sigma T &= f \quad \text{in } \Omega\,, \\ T &= g_D \ \text{ on } \Gamma_D\,, \\ \boldsymbol{w}\cdot\boldsymbol{n} &= g_N \ \text{ on } \Gamma_N\,, \end{aligned} \tag{18}$$

where Γ_D and Γ_N are, respectively, Dirichlet and Neumann parts of $\partial\Omega$, the boundary of Ω, and $\boldsymbol{n}$ is the outward unit normal to $\partial\Omega$. We assume that $\mathbf{K}$ is a symmetric positive definite diffusion tensor, $\mathbf{K}\in\mathbb{R}^{2\times 2}$, $\mathbf{K}=\mathbf{K}^T>0$, and σ is a given nonnegative function. Note that the source function f is not necessarily the same as in (1) and for non-stationary problems can include an additional term shown in (3).

To construct mesh Ω_h, we partition Ω into l polygonal mesh cells E_k with interfaces Γ_{st} between mesh cells E_s and E_t, $s<t$, and faces $\Gamma_{k,i}$ on the boundary $\partial\Omega$, $\Gamma_{k,i}\in\partial E_k\cap\partial\Omega$. We can write $\Omega=\bigcup_{k=1}^{l} E_k$.

Let E_k be a multi-material cell in Ω_h with its minimesh $E_{k,h}$. The minimesh $E_{k,h}$ is assumed to be a conforming polygonal mesh with fully established connectivity between its cells $e_{k,s}$, $s=\overline{1,l_k}$, which are also called material polygons. We discretize problem (18) on every cell $e_{k,s}$ using the mimetic finite difference (MFD) method and write the first two equations in the compact matrix-vector form:

$$\begin{aligned} M_s\overline{w}_s + B_s^T T_s + C_s^T\lambda_s &= 0\,, \\ B_s\overline{w}_s - \Sigma_s T_s &= -f_s \end{aligned} \tag{19}$$

as described in [24], where $\overline{w}_s$ is the vector of numerical fluxes on faces of $e_{k,s}$, T_s is the average of T over $e_{k,s}$, $\overline{\lambda}_s$ is the vector of face-based temperature unknowns on faces of $e_{k,s}$, and

$$\Sigma_s=\int_{e_{k,s}}\sigma\,dx\,,\quad f_s=\int_{e_{k,s}} f\,dx\,. \tag{20}$$

The Neumann boundary conditions are taken into account by setting the numerical fluxes $w_{s,i}$ corresponding to faces $\gamma_{k,s,i}$ of $e_{k,s}$ such that $\gamma_{k,s,i}\in\Gamma_N$ to

$$w_{s,i}=\frac{1}{|\gamma_{k,s,i}|}\int_{\gamma_{k,s,i}} g_N\,ds \tag{21}$$

and the Dirichlet boundary condition are taken into account by setting the components of $\overline{\lambda}_s$ corresponding to faces $\gamma_{k,s,j}$ of $e_{k,s}$ such that $\gamma_{k,s,j}\in\Gamma_D$ as follows:

$$\lambda_{s,j}=\frac{1}{|\gamma_{k,s,j}|}\int_{\gamma_{k,s,j}} g_D\,ds\,. \tag{22}$$

The first equation in (19) corresponds to the Fourier's (heat conduction) or Darcy's (flow in porous media) law and the second equation corresponds to the conservation of energy (heat conduction) or mass (flow in porous media) law. If $e_{k,s}$ and $e_{k,t}$ are two adjacent material polygons with a shared face $\gamma_{k,s,i}\equiv\gamma_{k,t,j}$, then the respective flux unknowns must satisfy the condition of flux conservation:

$$w_{s,i}+w_{t,j}=0. \tag{23}$$

Next, we express $\overline{w}_s$ in terms of $\overline{\lambda}_s$ and substitute the resulting expression into the left-hand side of the equation $C_s\overline{w}_s = C_s\overline{w}_s$ to obtain the following algebraic system:

$$S_s\overline{\lambda}_s = \overline{F}_s - C_s\overline{w}_s\,, \tag{24}$$

where

$$S_s = C_s M_s^{-1}\left(I - B_s^T(\Sigma_s + B_s M_s^{-1} B_s^T)^{-1} B_s M_s^{-1}\right) C_s^T\,. \tag{25}$$

Note that matrix M_s is SPD, matrix C_s is diagonal, and S_s is SPD if Σ_s is nonzero and symmetric semi-positive definite (SSPD) with the kernel consisting of the vector $\overline{e}_s$, where $\overline{e}_s$ is the vector of all ones, otherwise.

Let $\overline{\lambda}_k$ and $\overline{w}_k$ denote vectors of face-based temperature unknowns and unique numerical fluxes on faces of the minimesh $E_{k,h}$, including those on the boundary of Ω. Then we use the local assembling matrices $\mathcal{N}_s$ such that $\overline{\lambda}_s = \mathcal{N}_s\overline{\lambda}_k$ and condition (23) to obtain the algebraic system on the minimesh $E_{k,h}$:

$$S_k\overline{\lambda}_k = \overline{F}_k - C_k\overline{w}_k\,, \tag{26}$$

where

$$S_k = \sum_{s=1}^{l_k} \mathcal{N}_s^T S_s \mathcal{N}_s\,, \quad F_k = \sum_{s=1}^{l_k} \mathcal{N}_s^T \overline{F}_s\,. \tag{27}$$

Since the minimesh $E_{k,h}$ is face-connected, the matrix S_k is either SPD or SSPD with kernel $\overline{e}_k$ if σ is zero on E_k. Let us partition $\overline{\lambda}_k$ into $\overline{\lambda}_{k,int}$ and $\overline{\lambda}_{k,bnd}$ for temperature unknowns on interior and boundary faces of $E_{k,h}$ respectively. We do the same for the vector of numerical fluxes $\overline{w}_k$. Because the components of $\overline{\lambda}_k$ and $\overline{w}_k$ corresponding to the same face have the same index, we can write the corresponding matrices in the following block form,

$$S_k = \begin{pmatrix} S_{k,int} & S_{k,int,bnd} \\ S_{k,int,bnd}^T & S_{k,bnd} \end{pmatrix}, \quad C_k = \begin{pmatrix} 0 & 0 \\ 0 & C_{k,bnd} \end{pmatrix}. \tag{28}$$

Since $\overline{e}_k$ is the whole kernel of S_k, $S_{k,int}$ is an SPD matrix. Eliminating $\overline{\lambda}_{k,int}$ and $\overline{w}_{k,int}$ unknowns, we get the condensed algebraic system

$$\widetilde{S}_k\overline{\lambda}_{k,bnd} = \overline{\widetilde{F}}_k - \widetilde{C}_k\overline{w}_{k,bnd} \tag{29}$$

with matrices

$$\widetilde{S}_k = S_{k,bnd} - S_{k,int,bnd}^T S_{k,int} S_{k,int,bnd}, \quad \widetilde{C}_k = C_{k,bnd}\,. \tag{30}$$

Here, matrix $\widetilde{S}_k$ is either SPD or SSPD with the kernel consisting of vector $\overline{\widetilde{e}}_k$ of all ones, and matrix $\widetilde{C}_k$ is diagonal. For simplicity, we from now on denote $\overline{\lambda}_{k,bnd}$ by $\overline{\widetilde{\lambda}}_k$ and $\overline{w}_{k,bnd}$ by $\overline{\widetilde{w}}_k$.

Let the faces on the boundary of the minimesh $E_{k,h}$ be denoted by $\widetilde{\gamma}_{k,j}$, $j = \overline{1,\widetilde{n}_k}$. Currently, we have one unknown $\widetilde{\lambda}_{k,j}$ associated with every boundary face $\widetilde{\gamma}_{k,j}$.

We denote the faces of E_k, which are faces of the base mesh Ω_h, by $\Gamma_{k,s}$, $s = \overline{1,\widehat{n}_k}$, where every $\Gamma_{k,s}$ is a union of one of more faces $\widetilde{\gamma}_{k,j}$. We then make an assumption that the solution function is constant on every $\Gamma_{k,s}$, associate with every "base" face $\Gamma_{k,s}$ a single unknown $\widehat{\lambda}_{k,s}$, and assume that

$$\overline{\widetilde{\lambda}}_k = R_k\overline{\widehat{\lambda}}_k\,, \tag{31}$$

where $R_k \in \mathbb{R}^{\widetilde{n}_k \times \widehat{n}_k}$ has entries

$$r_{i,j} = \begin{cases} 1\,, & \gamma_{k,i} \in \Gamma_{k,j}\,, \\ 0\,, & \text{otherwise}\,, \end{cases} \tag{32}$$

and $\overline{\widehat{\lambda}}_k$ is the vector of all $\widehat{\lambda}_{k,s}$, $s = \overline{1,\widehat{n}_k}$.

Every face $\widetilde{\gamma}_{k,j}$ belongs to one and only one base face $\Gamma_{k,s}$ for some j and s, therefore every row of matrix R has one nonzero entry. On the other hand, every base face $\Gamma_{k,s}$ contains one of more faces $\widetilde{\gamma}_{k,j}$, so every column of R has at least one nonzero entry. This implies that the $\widetilde{n}_k \times \widehat{n}_k$ matrix R, where $\widehat{n}_k \le \widetilde{n}_k$, has exactly $\widehat{n}_k$ orthonormal rows and is therefore full rank.

Substituting $\overline{\widetilde{\lambda}}_k$ with $R_k\overline{\widehat{\lambda}}_k$ and multiplying by R_k^T from the left, we get a reduced algebraic system

$$\widehat{S}_k\overline{\widehat{\lambda}}_k = R_k^T\overline{\widetilde{F}}_k - R_k^T\widetilde{C}_k\overline{\widetilde{w}}_k \tag{33}$$

with a matrix

$$\widehat{S}_k = R_k^T \widetilde{S}_k R_k \,. \tag{34}$$

Let $\widehat{w}_{k,s}$ be the total flux through the face $\Gamma_{k,s}$, i.e.

$$|\Gamma_{k,s}|\widehat{w}_{k,s} = \sum_{\widetilde{\gamma}_{k,j}\in\Gamma_{k,s}} |\widetilde{\gamma}_{k,j}|\widetilde{w}_{k,j}\,, \tag{35}$$

let $\overline{\widehat{w}}_k$ be the vector of total fluxes $\widehat{w}_{k,s}$, and let $\widehat{C}_k$ be a diagonal matrix such that $(\widehat{C}_k)_{s,s} = |\Gamma_{k,s}|$. It follows that

$$\widehat{C}_k\overline{\widehat{w}}_k = R_k^T\widetilde{C}_k\overline{\widetilde{w}}_k\,, \tag{36}$$

and system (33) can be written as

$$\widehat{S}_k\overline{\widehat{\lambda}}_k = R_k^T\overline{\widetilde{F}}_k - \widehat{C}_k\overline{\widehat{w}}_k\,. \tag{37}$$

This means that the Neumann boundary conditions and the condition of flux conservation are now imposed on faces of the base mesh: if E_s and E_t are two adjacent cells of the base mesh with a shared face $\Gamma_{s,i}\equiv\Gamma_{t,j}$, then the respective flux unknowns must satisfy the following:

$$\widehat{w}_{s,i} + \widehat{w}_{t,j} = 0. \tag{38}$$

Note that for any $\overline{\widehat{v}}\in\mathbb{R}^{\widehat{n}_k}$ we have the corresponding vector $\overline{\widetilde{v}} = R_k\overline{\widehat{v}}\in\mathbb{R}^{\widetilde{n}_k}$ such that

$$\overline{\widetilde{v}}^T\widetilde{S}_k\overline{\widetilde{v}} = \overline{\widehat{v}}^T R_k^T\widetilde{S}_k R_k\overline{\widehat{v}} = \overline{\widehat{v}}^T\widehat{S}\overline{\widehat{v}}^T \tag{39}$$

and by construction of R_k it is full rank and if $\overline{\widetilde{v}} = \overline{\widetilde{e}}_k$, then $\overline{\widehat{v}} = \overline{\widehat{e}}_k$, the vector of all ones. Hence, the matrix $\widehat{S}_k$ is either SPD or SSPD with kernel $\overline{\widehat{e}}_k$ if $\sigma = 0$ on E_k.

Now, we use the assembling operators $\mathcal{N}_k$ such that $\overline{\widehat{\lambda}}_k = \mathcal{N}_k\overline{\lambda}$ to obtain the global algebraic system

$$S\overline{\lambda} = \sum_{k=1}^{l}\mathcal{N}_k^T R_k^T\overline{\widetilde{F}}_k - \sum_{k=1}^{l}\mathcal{N}_k^T\widehat{C}_k\overline{\widehat{w}}_k \tag{40}$$

with a matrix

$$S = \sum_{k=1}^{l}\mathcal{N}_k^T\widehat{S}_k\mathcal{N}_k\,. \tag{41}$$

Due to flux conservation condition (38) we have

$$\sum_{k=1}^{l}\mathcal{N}_k^T\widehat{C}_k\overline{\widehat{w}}_k = \overline{G}_N\,, \tag{42}$$

where $\overline{G}_N$ is a given vector of numerical fluxes on faces Γ_i of the base mesh Ω_h with the following components:

$$(G_N)_i = \begin{cases} -\int_{\Gamma_i} g_N\,ds & \text{if } \Gamma_i\in\Gamma_N\,,\\ 0\,, & \text{otherwise}\,. \end{cases} \tag{43}$$

Now, eliminating the known face-based temperatures on the Dirichlet part of the boundary, we obtain the global algebraic system with a matrix $\widehat{S}$. This matrix is SPD if $\sigma\neq 0$ on Ω, or if Ω_h is face-connected and Dirichlet part of the boundary is nonempty, $\Gamma_D\neq\emptyset$, as shown in [24].

Appendix B. Local matrices for the example in Section 4.3

Here, we use the example in Section 4.3 to show local matrices that result from discretizing problem (18) with methods described in Section 4.1 and Appendix A.

B.1. Homogenization methods

In the case of homogenization methods, we discretize the problem on the base cell E using the averaged parameters values. Let us denote the diffusion coefficient by k_*, where $k_* = k_H$ or $k_* = k_A$ for harmonic and arithmetic means respectively. The averaged value for σ in E is

$$\sigma_c = \frac{\sigma_1|e_1| + \sigma_2|e_2|}{|E|} = \frac{1}{2}(\sigma_1+\sigma_2)\,. \tag{44}$$

We denote the cell-average value of the solution by p_c, and when recovering the solution values in subcells e_1 and e_2 we set $p_1 = p_c = p_2$.

Then we use the mimetic finite differences to obtain the algebraic system of the same type as in (30) on cell E. The matrix blocks are as follows:

$$\begin{aligned} &W = \frac{h^2}{2k_*} I_4\,, \quad \Sigma = h^2\sigma_c\,, \\ &B = -h\begin{pmatrix}1 & 1 & 1 & 1\end{pmatrix}, \quad C = hI_4\,. \end{aligned} \tag{45}$$

Assuming that $\sigma = 0$ on E, the Schur-complement matrix for E that is used to assemble the global system according to (41) is

$$S = \frac{k_*}{2}\begin{pmatrix} 3 & -1 & -1 & -1 \\ -1 & 3 & -1 & -1 \\ -1 & -1 & 3 & -1 \\ -1 & -1 & -1 & 3 \end{pmatrix}. \tag{46}$$

B.2. ASC method

First, we use mimetic finite differences to obtain the algebraic system (30) on minimesh E_h. The matrices in (19) and (25) are

$$\begin{aligned} &W_s = \frac{h^2}{4k_s} I_4\,, \quad \Sigma_s = \frac{h^2}{2}\sigma_s\,, \\ &B_s = -\frac{h}{2}\begin{pmatrix}1 & 2 & 1 & 2\end{pmatrix}, \quad C_s = \frac{h}{2}\begin{pmatrix} 1 & 0 & 0 & 0 \\ 0 & 2 & 0 & 0 \\ 0 & 0 & 1 & 0 \\ 0 & 0 & 0 & 2 \end{pmatrix}, \\ &S_s = \frac{k_s}{20+\sigma_s h^2}\begin{pmatrix} 18+\sigma_s h^2 & -8 & -2 & -8 \\ -8 & 48+4\sigma_s h^2 & -8 & -32 \\ -2 & -8 & 18+\sigma_s h^2 & -8 \\ -8 & -32 & -8 & 48+4\sigma_s h^2 \end{pmatrix}, \end{aligned} \tag{47}$$

$s = 1, 2$. Then, we introduce new DOF's $\widehat{\lambda}_s$, $s = \overline{1,4}$, assuming that $\widetilde{\lambda}_1 = \widehat{\lambda}_1 = \widetilde{\lambda}_2$, $\widetilde{\lambda}_3 = \widehat{\lambda}_2$, $\widetilde{\lambda}_4 = \widehat{\lambda}_3 = \widetilde{\lambda}_5$, and $\widetilde{\lambda}_6 = \widehat{\lambda}_4$. The matrix corresponding to R_k in (31) is as follows:

$$R = \begin{pmatrix} 1 & 0 & 0 & 0 \\ 1 & 0 & 0 & 0 \\ 0 & 1 & 0 & 0 \\ 0 & 0 & 1 & 0 \\ 0 & 0 & 1 & 0 \\ 0 & 0 & 0 & 1 \end{pmatrix} \tag{48}$$

Let us assume that $\sigma = 0$ on E, then the Schur-complement matrix corresponding to $\widehat{S}_k$ in (34) is

$$\widehat{S} = \frac{1}{15}\begin{pmatrix} 25k_A & -10k_1 & -5k_A & -10k_2 \\ -10k_1 & 20k_1+8k_H & -10k_1 & -8k_H \\ -5k_A & -10k_1 & 25k_A & -10k_2 \\ -10k_2 & -8k_H & -10k_2 & 20k_2+8k_H \end{pmatrix}. \tag{49}$$

References

[1] T. Arbogast, G. Pencheva, M.F. Wheeler, I. Yotov, A multiscale mortar mixed finite element method, Multiscale Model. Simul. 6 (1) (2007) 319–346.

[2] H.-T. Ahn, M. Shashkov, Multi-material interface reconstruction on generalized polyhedral meshes, J. Comput. Phys. 226 (2) (2007) 2096–2132.

[3] C. Annavarapu, M. Hautefeuille, J.E. Dolbow, A robust Nitsche's formulation for interface problems, Comput. Methods Appl. Mech. Eng. 225–228 (2012) 44–54.

[4] A. Barlow, R. Hill, M. Shashkov, Constrained optimization framework for interface-aware sub-scale dynamics closure model for multi-material cells in Lagrangian and arbitrary Lagrangian–Eulerian hydrodynamics, J. Comput. Phys. 276 (1) (2014) 92–135.

[5] A.J. Barlow, P.-H. Maire, W.J. Rider, R.N. Rieben, M.J. Shashkov, Arbitrary Lagrangian–Eulerian methods for modeling high-speed compressible multi-material flows, J. Comput. Phys. 322 (1) (2016) 603–665.

[6] E. Burton, Lagrangian Hydrodynamics in the FLAG Code, Technical Report LA-UR-07-7547, Los Alamos National Laboratory, 2007, available at https://www.researchgate.net/publication/237101823.

[7] D.J. Benson, Computational methods in Lagrangian and Eulerian hydrocodes, Comput. Methods Appl. Mech. Eng. 99 (2–3) (1992) 235–394.
[8] F. Brezzi, M. Fortin, Mixed and Hybrid Finite Element Methods, Springer-Verlag, Berlin, Heidelberg, 1991.
[9] E. Burman, S. Claus, P. Hansbo, M.G. Larson, A. Massing, CutFEM: discretizing geometry and partial differential equation, Int. J. Numer. Methods Eng. 104 (2015) 472–501.
[10] A.S. Dawes, Solving the diffusion equation on a non-aligned mesh, Comput. Fluids 83 (2013) 77–89.
[11] A.S. Dawes, C.M. Malone, M.J. Shashkov, Some New Verification Test Problems for Multi-Material Diffusion on Meshes That Are Non-aligned with Material Boundaries, Technical Report LA-UR-16-24696, Los Alamos National Laboratory, 2016.
[12] J. Dolbow, S. Mosso, J. Robbins, T. Voth, Coupling volume-of-fluid based interface reconstructions with the extended finite element method, Comput. Methods Appl. Mech. Eng. 197 (5) (2008) 439–447.
[13] V. Dyadechko, M. Shashkov, Reconstruction of multi-material interfaces from moment data, J. Comput. Phys. 227 (11) (2008) 5361–5384.
[14] L.J. Durlofsky, Accuracy of mixed and control volume finite element approximations to Darcy velocity and related quantities, Water Resour. Res. 30 (4) (1994) 965–973.
[15] B. Ganis, I. Yotov, Implementation of a mortar mixed finite element method using a multiscale flux basis, Comput. Methods Appl. Mech. Eng. 198 (2009) 3989–3998.
[16] R.V. Garimella, K. Lipnikov, Solution of the diffusion equation in multi-material domains by sub-division of elements along reconstructed interfaces, Int. J. Numer. Methods Fluids 65 (2011) 1423–1437.
[17] A. Hansbo, P. Hansbo, An unfitted finite element method, based on Nitsche's method, for elliptic interface problems, Comput. Methods Appl. Mech. Eng. 191 (2002) 5537–5552.
[18] U. Hornung (Ed.), Homogenization and Porous Media, Springer, 1996.
[19] J. Hyman, M. Shashkov, S. Steinberg, The numerical solution of the diffusion problems in strongly heterogeneous non-isotropic materials, J. Comput. Phys. 132 (1997) 130–148.
[20] E. Kikinzon, Yu. Kuznetsov, M.J. Shashkov, New Algorithm for Solving Multi-Material Diffusion Problems on Mesh Non-aligned with Material Interfaces, Technical Report LA-UR-16-21548, Los Alamos National Laboratory, 2016.
[21] Yu. Kuznetsov, S. Repin, New mixed finite element method on polygonal and polyhedral meshes, Russ. J. Numer. Anal. Math. Model. 18 (2003) 261–278.
[22] Yu.A. Kuznetsov, Mixed finite element methods on polyhedral meshes for diffusion equations, in: R. Glowinski, P. Neittaanmaki (Eds.), Partial Differential Equations: Modelling and Numerical Simulation, Springer, The Netherlands, 2008, pp. 27–42.
[23] K. Lipnikov, G. Manzini, M. Shashkov, Mimetic finite difference method, J. Comput. Phys. B 257 (15) (2014) 1163–1227.
[24] K. Lipnikov, G. Manzini, D. Svyatskiy, Analysis of the monotonicity conditions in the mimetic finite difference method for elliptic problems, J. Comput. Phys. 230 (7) (2011) 2620–2642.
[25] J.E. Morel, R.M. Roberts, M.J. Shashkov, A local support-operators diffusion discretization scheme for quadrilateral $r-z$ meshes, J. Comput. Phys. 144 (1998) 117–151.
[26] G. Pencheva, I. Yotov, Balancing domain decomposition for mortar mixed finite element methods, Numer. Linear Algebra Appl. 10 (2003) 159–180.
[27] J. Pouderoux, M. Berndt, M. Kenamond, M. Shashkov, ShaPo: a framework for generating 2D Voronoi meshes, Presented at Multimat 2015 Conference, Germany. Available at https://www.researchgate.net/publication/281811618.
[28] W.J. Rider, D.B. Kothe, Reconstructing volume tracking, J. Comput. Phys. 141 (2) (1998) 112–152.